Computer Modeling in Engineering & Sciences

Tech Science Press

https://doi.org/10.32604/cmes.2026.083537

ARTICLE

Machine Learning Prediction of the Compressive Strength of Nano-Silica-Modified Hybrid Geopolymer Mortar

Soran Manguri[1,2], Kasim Mermerdaş[1], Briar Esmail[3,4] and Ahmed Manguri[2,*]

[1]Civil Engineering Department, Engineering Faculty, Harran University, Şanlıurfa, Türkiye
[2]Civil Engineering Department, College of Engineering, University of Raparin, Rania, Iraq
[3]Department of Civil Engineering, Faculty of Engineering, Koya University, Koya, Iraq
[4]ISISE, Department of Civil Engineering, University of Minho, Azurém, Guimarães, Portugal

*Corresponding Author: Ahmed Manguri. Email: ahmed.manguri@uor.edu.krd

Received: 06 April 2026; Accepted: 27 May 2026; Published: 30 June 2026

ABSTRACT: Geopolymer materials are increasingly recognized as sustainable alternatives to conventional cementitious materials due to their lower environmental impact and promising engineering performance. Recent studies have demonstrated that incorporating nanomaterials can further enhance the properties of geopolymer systems. In particular, nano-silica has been reported to significantly improve the mechanical performance of geopolymer materials. However, accurate prediction of compressive strength remains challenging because of the complex nonlinear interactions among mix design parameters, activator chemistry, and curing conditions. This study develops a machine learning framework to predict the 28-day compressive strength of nanosilica-modified hybrid geopolymer mortar using a dataset of 73 mixes compiled from the literature. Five regression models, Linear Regression, Random Forest, CatBoost, Extreme Gradient Boosting, and Extra Trees Regressor, were benchmarked using 10-fold cross-validation and 100 repeated Monte Carlo simulations. The three best baseline-performing models, namely Extra Trees Regressor, CatBoost, and Random Forest, were then optimized using Bayesian hyperparameter tuning with the Optuna framework and Tree-structured Parzen Estimator sampler across 200 optimization trials. The optimized Extra Trees Regressor achieved the best performance, with R^2 values of 0.906 and 0.844, RMSE values of 5.43 and 6.24 MPa under 10-fold cross-validation and Monte Carlo simulation, respectively. Feature-importance analysis showed that binder composition, including slag, fly ash, and metakaolin contents, was the dominant factor, contributing more than 50% of the model importance, followed by nano-silica dosage at approximately 15%. While NaOH molarity, alkaline activator content, and curing conditions exhibited comparatively lower influence, their contributions remained consistent with established geopolymerization mechanisms. In addition, the optimized model was deployed as an open-access web-based prediction tool to support practical strength estimation and mix-design decision-making.

KEYWORDS: Geopolymer mortar; nano-silica; machine learning; modeling; mix design optimization

1 Introduction

Concrete remains the most widely used construction material in modern infrastructure due to its versatility, mechanical strength, and economic feasibility. However, the primary binder used in concrete, ordinary Portland cement (OPC), is associated with considerable environmental challenges. The production of cement involves energy-intensive processes and the calcination of limestone, which results in substantial carbon dioxide emissions. The cement industry is estimated to contribute approximately 7%–8% of global anthropogenic CO_2 emissions, making it one of the largest industrial sources of greenhouse gases [1–3].

Copyright © 2026 The Authors. Published by Tech Science Press. This work is licensed under a Creative Commons Attribution 4.0 International License, which permits unrestricted use, distribution, and reproduction in any medium, provided the original work is properly cited.

With growing concerns about environmental sustainability and climate change, researchers have been actively exploring alternative binder systems to reduce the environmental footprint of conventional cementitious materials. Among the most promising alternatives are alkali-activated materials and geopolymers, which have gained significant attention due to their lower carbon emissions, excellent chemical resistance, and favorable mechanical performance [4–6].

Geopolymers are inorganic aluminosilicate polymeric materials produced through the alkaline activation of silica- and alumina-rich precursor materials such as fly ash [7,8], ground granulated blast furnace slag [9,10], and metakaolin [11,12]. When these aluminosilicate materials react with alkaline activating solutions, they undergo a dissolution, transportation, and polycondensation reactions that lead to the formation of a three-dimensional aluminosilicate network commonly referred to as geopolymer gel [13–15]. The resulting geopolymeric structure typically consists of sodium aluminosilicate hydrate (N-A-S-H) or calcium aluminosilicate hydrate (C-A-S-H) gel, depending on the precursor composition. These gel structures contribute significantly to the mechanical strength and durability of geopolymer materials [16].

Within geopolymer systems, geopolymer mortar, which consists of geopolymer binder combined with fine aggregates and alkaline activating solutions, represents an important material for both structural and repair applications. The properties of geopolymer mortar are influenced by several parameters, including precursor composition, curing temperature, mixture proportions, and the type and concentration of alkaline activators [17]. In most geopolymer systems, alkaline activation is achieved using sodium hydroxide (NaOH) and sodium silicate (Na_2SiO_3) solutions. The NaOH molarity controls the dissolution of aluminosilicate species and the availability of reactive silica and alumina required for geopolymerization. Higher NaOH molarity generally enhances geopolymeric gel formation and compressive strength [18]. Although excessive concentrations may reduce workability and cause undesirable microstructural changes. In addition, the Na_2SiO_3/NaOH ratio influences the availability of soluble silica, while sodium silicate enhances polymerization and contributes to a denser and more stable geopolymer matrix [19–21].

In recent years, nanotechnology has been increasingly applied in cementitious and geopolymer materials to improve their mechanical and durability properties. Nanoparticles possess extremely small particle sizes and high specific surface areas, which allow them to act as nucleation sites for reaction products, refine pore structures, and improve the microstructural characteristics of the binder matrix. Various nanoparticles, including nano-TiO_2, nano-Al_2O_3, nano-clay, carbon nanotubes, and nano-silica, have been investigated in cementitious composites to enhance their mechanical performance and durability [22].

Among the different types of nanoparticles investigated in geopolymer systems, nano-silica (NS) has attracted particular attention due to its extremely high surface area, high pozzolanic reactivity, and ability to significantly improve the microstructure of cementitious and geopolymer matrices [23]. Nano-silica can accelerate the geopolymerization process by providing nucleation sites for the formation of geopolymeric gels, while also filling micro-voids within the matrix and improving particle packing density [24]. As a result, the incorporation of nano-silica has been shown to enhance the compressive strength, reduce porosity, and improve the durability of geopolymer composites [25]. Several recent studies have reported that small additions of nano-silica significantly enhance the mechanical performance of geopolymer mortars due to improved gel formation and microstructural refinement [26].

The incorporation of nano-SiO_2 improves the mechanical properties and durability of geopolymer mortar by producing a denser microstructure and refined interfacial zones [26]. Among the various mechanical properties of geopolymer mortar and concrete, compressive strength is widely considered the most important indicator of structural performance. Compressive strength reflects the load-bearing capacity of a material and is a fundamental parameter in the design and evaluation of structural elements.

In cementitious and geopolymer materials, the 28-day compressive strength is commonly used as the standard indicator for evaluating the long-term mechanical performance of the material [27].

In addition to experimental investigations, predictive modeling techniques have recently gained considerable attention in the field of cementitious and geopolymer materials. Modeling approaches enable researchers to analyze complex relationships among mixture parameters and develop a credible model for forecasting compressive strength (CS). This is critical for saving time, energy, and money while also providing guidance for scheduling the construction process and removing formwork. Various modeling techniques have been applied for predicting the compressive strength of geopolymer materials, including linear regression (LR), nonlinear regression NLR and multi-logistic regression models MLR [28,29] and an artificial neural network (ANN) [29]. Artificial Neural Network-based models, particularly Deep Neural Networks, have also been found to reliably predict. This provides a powerful tool to model complex relationships in advanced complex cementitious materials such as geopolymer composites [30].

This study presents a novel machine learning framework for predicting the 28-day compressive strength of nano-silica–modified geopolymer mortar. Current literature indicates that predictive machine learning models for nano-silica–modified geopolymer mortar systems remain insufficiently explored. Although previous studies have applied statistical and machine learning techniques to geopolymer materials, most studies focused on conventional geopolymer binders, adopted single-model approaches with limited validation, or lacked rigorous validation procedures. To address this research gap, a comprehensive dataset comprising 73 experimental mixtures was compiled from the literature and used to develop and evaluate five machine learning algorithms, namely Linear Regression (LR), Random Forest (RF), CatBoost, Extreme Gradient Boosting (XGBoost), and Extra Trees Regressor (ETR). Furthermore, the three best-performing models (ET, CatBoost, and RF) were optimized using Bayesian hyperparameter optimization through the Optuna framework with the Tree-structured Parzen Estimator (TPE) sampler over 200 optimization trials. Unlike previous studies, the proposed framework integrates a dual-validation strategy combining 10-fold cross-validation and Monte Carlo simulation to enhance prediction robustness and generalization capability. In addition, feature importance analysis was conducted to identify the key parameters governing compressive strength, and a practical web-based tool was developed for real-time prediction of nano-silica–modified geopolymer mortar strength. The compiled dataset and corresponding mixture parameters are summarized in Table 1.

Table 1: Summary of the constituents of geopolymer mortar mixes reported in the literature.

Ref.	A/B	B (kg/m^3)	FA (kg/m^3)	SH (kg/m^3)	SS (kg/m^3)	Molarity	SS/SH	Ns (kg/m^3)	T (°C)	CS (MPa)
[31]	0.4	450–500	1500	72.73	127.27	8–12	1.75	0–50	27–60	14.04–42.8
[32]	0.4	711–734	1173	97.78	195.56	8	2	0–21.3	20	19–59
[33]	0.3	1100	860	108	223	3	2.06	0–11	28	62.2–70.2
[34]	0.5	686–700	1033.5	100	250	12	2.5	0–14	23	66–74
[25]	0.4	714.2–723.8	1086.2	82.76	206.9	8	2.5	0–28.6	25	12.8–27.4
[35]	0.5	637–650	1040	92.9–130	195–232.1	12	1.5–2.5	0–13	23	44–70
[36]	0.6	460.61	1463	78.96	197.41	10	2.5	0–9.2	25	38–80
[36]	0.6	460.61	1463	78.96	197.41	10	2.5	0–9.2	60	42–82
[37]	0.7	450	1125	105	210	8–12	2	18	23–70	39–54
[38]	0.35	650	1300	65	163	10	2.5	13	27–60	31–69
[39]	0.5	432–450	432–450	64.28	160.71	16	2.5	0–17.3	25	19.7–28.3
Min.	0.3	432	432	64.28	127.27	3	1.5	0	20	12.8
Max.	0.7	1100	1500	130	250	16	2.5	50	70	82
St.Div.	0.1	154.78	281.26	17.01	35.07	2.6	0.34	12.46	14.97	17.79

2 Background and Data Compilation

To develop the predictive model for compressive strength, a dataset was compiled from previously published experimental studies on nano-silica-modified geopolymer mortar. Only studies reporting detailed mixture compositions and corresponding compressive strength values were considered. These studies provide the experimental data used to construct the modelling dataset and represent a wide range of mixture parameters, curing conditions, and nano-silica dosages. Early experimental studies showed that nano-silica significantly enhances compressive strength when used in small quantities. For example, an optimum nano-silica dosage of approximately 1.5% by weight of binder was reported to increase the 28-day compressive strength by nearly 95% compared with the control mixture. However, higher nano-silica contents may lead to particle agglomeration and reduced workability, thereby negatively affecting compressive strength [36].

Adak et al. [31] investigated the influence of nano-silica on fly ash-based geopolymer mortar under ambient curing conditions. Nano-silica was incorporated at dosages ranging from 0% to 10%, and the results showed that compressive strength increased with nano-silica addition up to 6%, achieving an improvement of approximately 16% compared with the control mixture. Beyond this dosage, compressive strength decreased due to nanoparticle agglomeration and increased water demand.

Deb et al. [32] studied ambient-cured fly ash geopolymer mortar incorporating 3% nano-silica and reported a compressive strength improvement of approximately 10%–20% compared with the control mixture. The enhancement was mainly associated with reduced porosity and the nucleation effect of nano-silica particles, which accelerate geopolymerization reactions and improve gel formation. Prakasam et al. [33] evaluated FA/GGBS-based geopolymer mortar containing nano-silica at 1% and 2% by weight of fly ash. Their results showed that compressive strength increased with the addition of nano-silica, reaching its highest value at 2% nano-silica, representing an improvement of approximately 12% over the control mixture. This increase was mainly attributed to additional N-A-S-H gel formation and improved microstructural densification.

Rathinam et al. [25] investigated geopolymer mortar produced from fly ash and GGBFS, with nano-silica contents ranging from 0% to 4%. Their results indicated that compressive strength increased with the addition of nano-silica and reached an optimum at 1% nano-silica, with strength improving by approximately 30% compared with the reference mixture. Higher nano-silica contents slightly reduced strength due to poor nanoparticle dispersion and reduced workability. Studies on metakaolin-based geopolymer systems have also confirmed the positive influence of nano-silica. Kamal et al. investigated nano-silica dosages ranging from 1% to 4% under both ambient and hot curing conditions. Their results showed that 3% nano-silica significantly improved compressive strength, achieving increases of approximately 110% under ambient curing and 95% under hot curing conditions [39].

Despite the clear advantages of incorporating nano-silica, excessive nano-silica content can adversely affect compressive strength. Selvarajan and Paramasivam [36] reported that nano-silica improved the mechanical properties of geopolymer mortar up to a certain limit, but when the nano-silica content exceeded approximately 2%, the compressive strength began to decline. This reduction was mainly related to poor dispersion and nanoparticle clustering within the mixture, which created weak zones in the geopolymer matrix. Moreover, the high surface area of nano-silica increased water demand, thereby reducing workability and affecting the mixture's homogeneity, ultimately resulting in lower compressive strength.

Gökçegöz et al. [37] investigated the combined influence of nano-silica and NaOH molarity on MK–GGBFS geopolymer mortar. Nano-silica was incorporated at 4%, while NaOH molarity varied between 4, 8, and 12 M. Their results showed that increasing molarity improved compressive strength due to enhanced dissolution of aluminosilicate precursors. At 8 M NaOH, compressive strength increased from 39 to 46 MPa, whereas at 12 M NaOH, it increased from 49 to 54 MPa with the addition of nano-silica.

Overall, the reviewed studies consistently indicate that nano-silica enhances the compressive strength of geopolymer mortar when used in small dosages, typically within the range of 1% to 3% by weight of binder. The improvement is primarily attributed to enhanced geopolymerization, pore refinement, and microstructural densification. However, higher nano-silica contents tend to reduce strength due to particle agglomeration, increased water demand, and reduced workability. In addition, curing conditions and alkaline activator concentration significantly influence strength development, with higher molarity generally promoting improved performance. These findings highlight the complex interactions among mixture parameters and justify the need for advanced predictive modeling approaches.

3 Modeling Phase

3.1 Statistical Assessment

Detailed information about each variable input parameter used in the model is presented in Sections 3.1.1–3.1.9. While Table 2 shows some statistical characteristics of the collected datasets. A histogram was created to illustrate the frequency distribution pattern of the continuous material property datasets. This visualization helps examine the data's distribution characteristics (such as normality), as well as identify potential outliers and any skewness [28]. Additionally, statistical criteria including standard deviation, variance, skewness, and kurtosis were computed to describe the distribution of each variable in relation to compressive strength. Kurtosis is a statistical measure that reflects the extent to which the tails of a data distribution differ from those of a normal distribution. It indicates the heaviness of the distribution tails, whereas skewness represents the symmetry of the distribution. In contrast, skewness measures the degree to which a distribution deviates from a normal distribution. For example, a skewness value of zero represents a normal distribution, while a right skew corresponds to a lognormal distribution. Furthermore, variance describes the level of dispersion within the dataset; a larger spread in the data results in a higher variance around the mean [40].

Table 2: Summary of statistical analysis of input model parameters.

Model Parameters	No. of Data	Average	Median	St.Div.	Min.	Max.	Variance	Skewness	Kurtosis
A/B	73	0.45	0.4	0.1	0.3	0.7	0.01	0.92	0
B (kg/m^3)	73	598.55	643.5	152.85	432	1100	23,363.18	1.25	2.31
Fly ash	58	388.16	465	243.89	0	734	59,480.96	−0.3	−1.49
Slag	47	405.74	368.49	204.25	71.42	650	41,717.38	−0.34	−1.24
Cement	4	73.33	73.33	0	73.33	73.33	0	0	0
Metakaolin	9	345	432	113.95	225	450	12,985.31	−0.26	−2.56
FA (kg/m^3)	73	1209.08	1173	281.26	432	1500	79,109.06	−1.23	1.56
SH (kg/m^3)	73	84.27	78.96	17.01	64.28	130	289.45	0.78	0.09
SS (kg/m^3)	73	181.35	195.56	35.07	127.27	250	1229.78	−0.21	−0.81
M	73	9.9	10	2.6	3	16	6.75	0.1	1.62
SS/SH	73	2.18	2.06	0.34	1.5	2.5	0.12	−0.35	−1.43
Ns (kg/m^3)	73	13.55	13	12.46	0	50	155.24	1.31	1.63
T (°C)	73	31.48	25	14.97	20	70	224	1.54	0.67
CS (MPa)	73	43.43	42	17.79	12.87	82	316.44	0.23	−0.82

3.1.1 The Alkaline Solution to Binder Ratio (A/B)

The alkaline solution represents the total amount of alkaline activator used to activate the source binder materials, including both sodium silicate and sodium hydroxide solutions at the required molarities. Based on the collected datasets, the A/B ratio of the GPM mixtures modified with Ns ranged from 0.3 to 0.7, with a mean value of 0.45 and a standard deviation of 0.1. Furthermore, the statistical analysis indicated that the

variance was 0.01, the skewness was 0.88, and the kurtosis was 0. Fig. 1 presents the relationship between CS and A/B, along with histograms illustrating the distribution of GPM mixtures incorporating Ns.

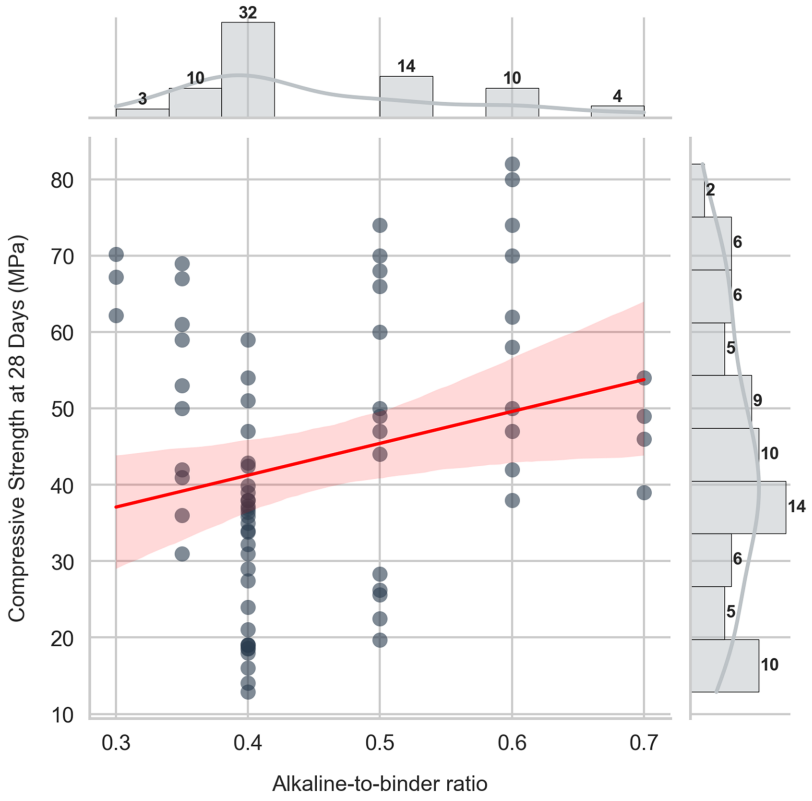

Figure 1: Marginal plot between CS and A/B content of GPM mixtures incorporated Ns.

3.1.2 Binder Content (B)

Fly ash, GGBFS, and MK are among the primary materials used by researchers as binder sources in the production of GPM composites. Based on the collected datasets, the binder content ranged from 432 to 1100 kg/m^3, with a mean of 599.75 kg/m^3 and a standard deviation of 152.85 kg/m^3. In addition, statistical evaluation of the dataset showed that the variance, skewness, and kurtosis were 23,363.18, 1.23, and 2.39, respectively. Fig. 2 illustrates the relationship between CS and binder (b) content, along with the frequency distribution of the collected data for GPC mixtures incorporated with Ns.

3.1.3 Fine Aggregate Content (FA)

Natural and crushed sands were used as fine aggregates (FA) in GPM mixtures, as in conventional concrete mixtures. The fine aggregate properties in the compiled dataset were obtained from studies in which materials generally conform to ASTM C33 requirements. Based on datasets from the reviewed literature, the FA content ranged from 432 to 1500 kg/m^3, with a mean of 1204.57 kg/m^3 and a standard deviation of 278.79 kg/m^3. Additional details regarding other statistical assessment parameters and correlations between CS and SH content are presented in Fig. 3.

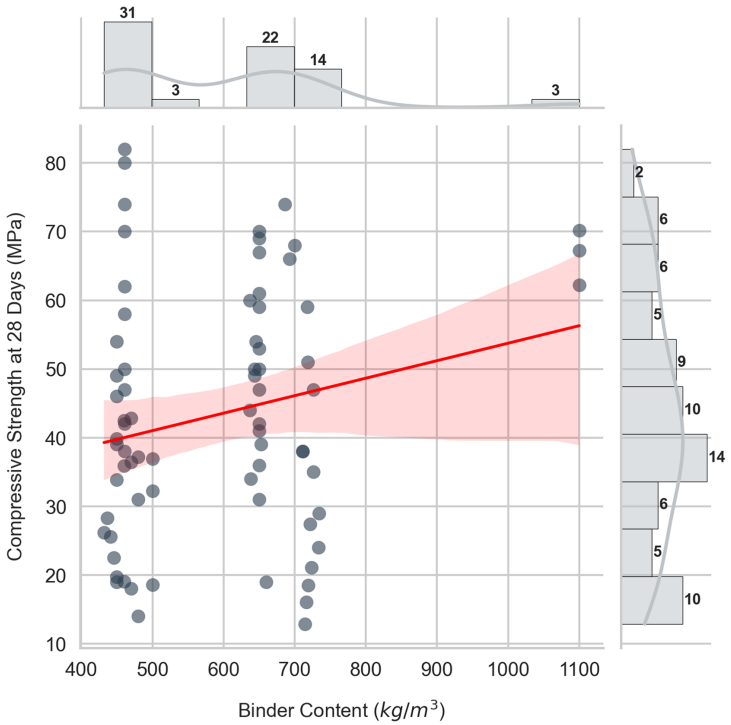

Figure 2: Marginal plot between CS and Binder content of GPM mixtures incorporated Ns.

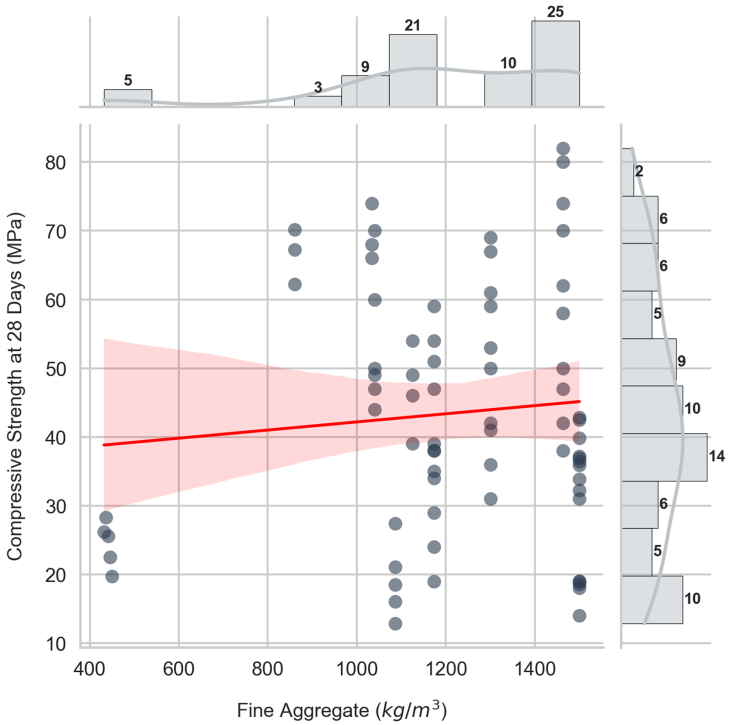

Figure 3: Marginal plot between CS and FA of GPM mixtures incorporated Ns.

3.1.4 NaOH Content (SH)

Sodium hydroxide (SH) is commonly available in solid form as pellets or flakes, typically with a purity greater than 97%. It is dissolved in the required amount of water to prepare an SH solution with the desired molarity. Based on the datasets collected in this study, the SH content in 1 m^3 of GPM mixtures incorporating Ns ranged from 64.28 to 130 kg/m^3, with a mean of 84.5 kg/m^3 and a standard deviation of 16.84 kg/m^3. Further details regarding other statistical assessment parameters, as well as the correlation between CS and SH content, can be found in Fig. 4.

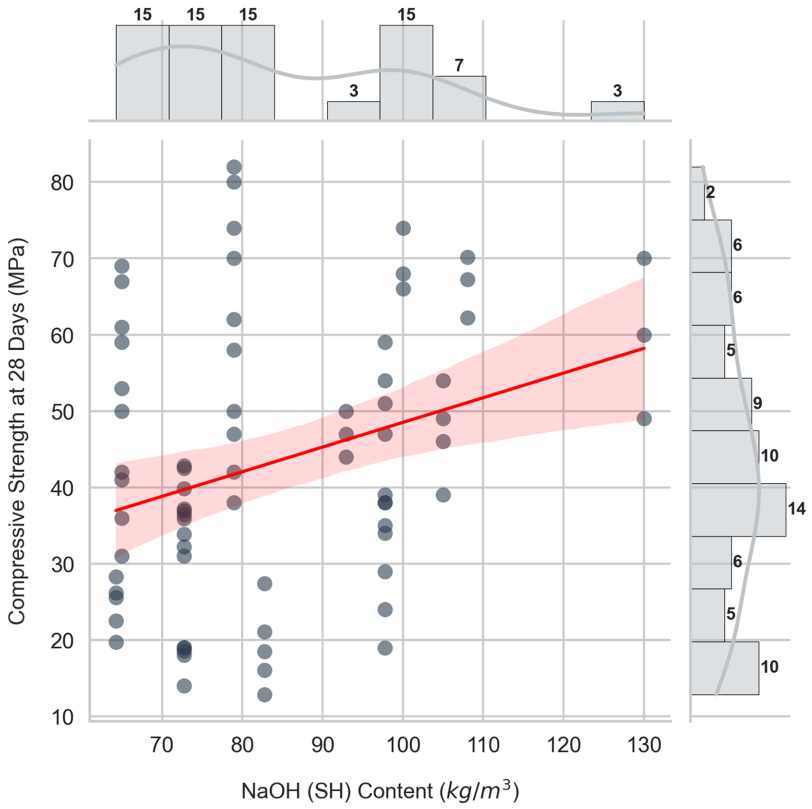

Figure 4: Marginal plot between CS and NaOH content of GPM mixtures incorporated Ns.

3.1.5 Na_2SiO_3 Content (SS)

Water glass, also known as sodium silicate (SS), is a liquid alkaline activator primarily composed of Na_2O, SiO_2, and H_2O. Based on previously reported studies on GPM mixtures incorporating Ns, the SS content ranged from 127.27 to 250 kg/m^3, with a mean value of 182.7 kg/m^3 and a standard deviation of 35.6 kg/m^3. Moreover, the relationship between CS and SS content in GPM mixtures is illustrated in Fig. 5.

3.1.6 Molarity (M)

In GPM research, the concentration of sodium hydroxide (SH) dissolved in water is expressed in terms of molarity (M). Based on the datasets collected from the reviewed studies, the molarity of SH ranged from 3 to 16 M, with a mean value of 9.96 M and a standard deviation of 2.59 M. Furthermore, the statistical analysis of the compiled datasets indicated that the variance, skewness, and kurtosis were 6.69, 0.05, and 1.58, respectively. The relationship between CS and M, along with the frequency distribution of the GPM datasets incorporated with Ns, is shown in Fig. 6.

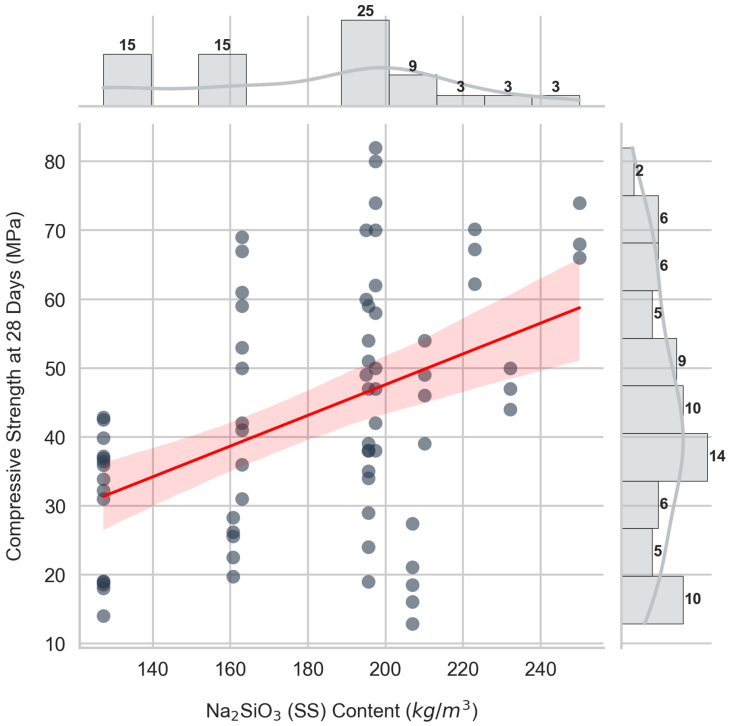

Figure 5: Marginal plot between CS and Na_2SIO_3 content of GPM mixtures incorporated Ns.

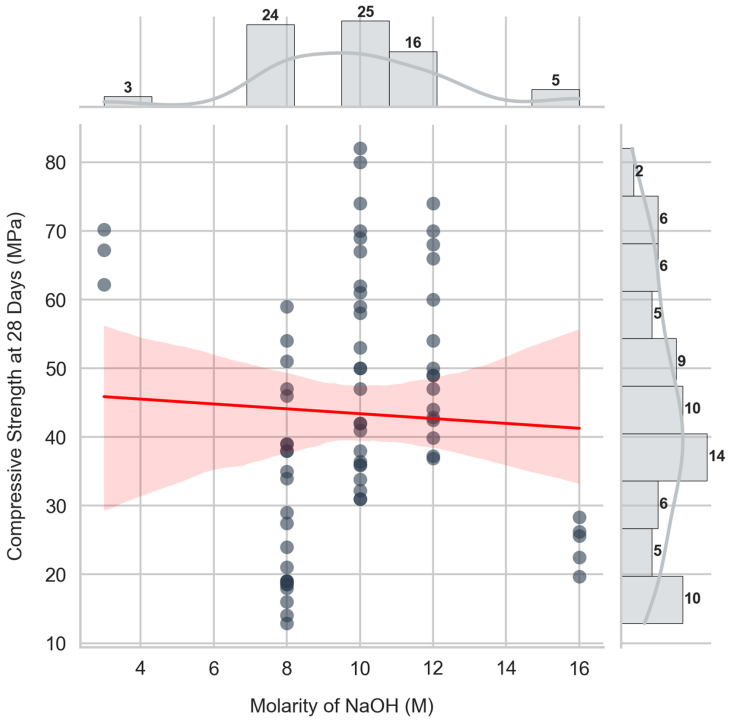

Figure 6: Marginal plot between CS and molarity of NaOH of GPM mixtures incorporated Ns.

3.1.7 Na_2SiO_3/NaOH (SS/SH)

This parameter represents the ratio of sodium silicate (SS) to sodium hydroxide (SH) in the alkaline activator solution prepared at the required molarity. Typically, the SS/SH solution is prepared approximately 24 h prior to mixing the GPM constituents to ensure proper dissolution and stabilization. Based on the collected datasets, the SS/SH ratio ranged from 1.5 to 2.5, with a mean value of 2.19 and a standard deviation of 0.34. Furthermore, the relationship between CS and the SS/SH ratio, together with the frequency distribution of the corresponding datasets, is presented in Fig. 7.

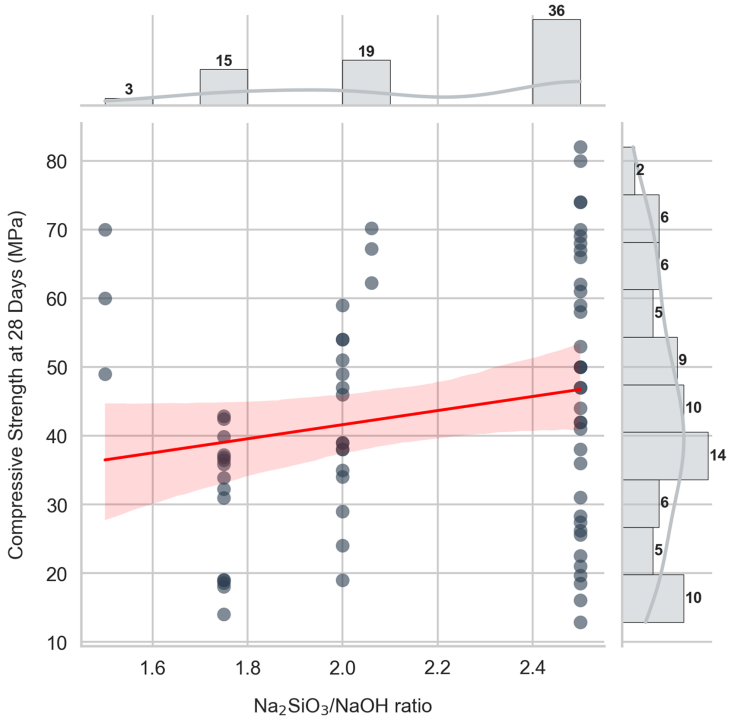

Figure 7: Marginal plot between CS and Na_2SIO_3/NaOH of GPM mixtures incorporated Ns.

3.1.8 Nano-Silica Content (Ns)

As discussed earlier, Ns is the most commonly utilized nanoparticle (NP) by researchers to enhance the various properties of GPM composites. It is typically incorporated either as a binder replacement or as an additive in the mixture. Based on the compiled datasets, the Ns content used to improve GPM composites ranged from 0 to 50 kg/m^3, with a mean value of 13.36 kg/m^3 and a standard deviation of 12.39 kg/m^3. In addition, further statistical evaluation parameters, along with the correlation between CS and Ns content, are shown in Fig. 8.

3.1.9 Curing Temperature

Ambient and oven curing regimes are commonly used to cure GPM composites. One of the primary motivations for incorporating nanoparticles (NPs) into GPM mixtures is to facilitate a transition from oven curing toward ambient curing conditions. Based on the compiled datasets, GPM specimens modified with Ns were cured at temperatures ranging from 23°C to 70°C, with a mean curing temperature of 31.31°C and a standard deviation of 14.8°C. Furthermore, statistical evaluation indicated that the dataset's variance,

skewness, and kurtosis were 219.05, 1.58, and 0.81, respectively. The variation of CS with Ns content, along with the frequency distribution of the Ns datasets, is illustrated in Fig. 9.

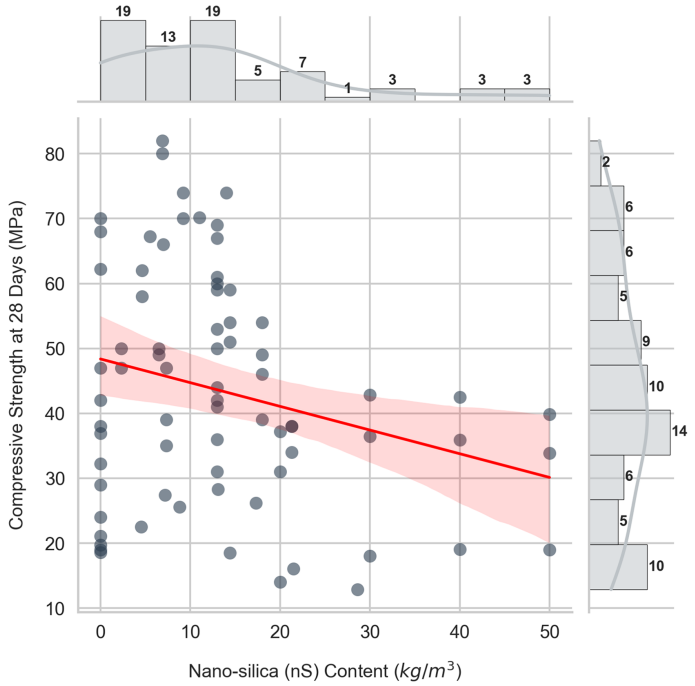

Figure 8: Marginal plot between CS and Ns content of GPM mixtures incorporated Ns.

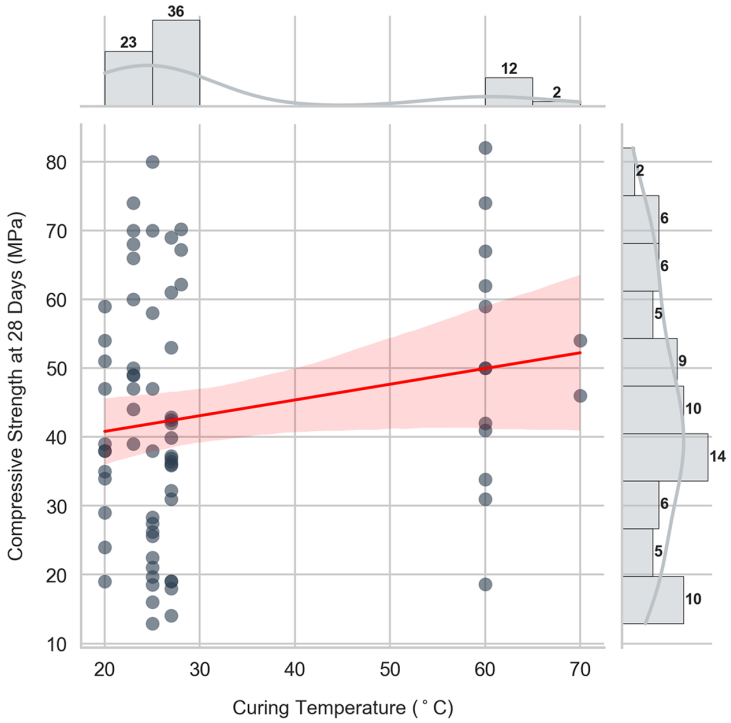

Figure 9: Marginal plot between CS and curing content of GPM mixtures incorporated with Ns.

4 Model Development and Statistical Validation

4.1 Dataset Preparation and Preprocessing

The predictive modeling framework was developed using an experimental dataset comprising 73 geopolymer mortar mixtures. Prior to model development, the dataset was carefully prepared to ensure reliable learning by the machine learning algorithm. Nine input variables were selected based on their known influence on the geopolymerization process and compressive strength development. These variables included molarity of the alkaline solution (M), binder components (fly ash, slag, and metakaolin), fine aggregate content (FA), nano-silica dosage (Ns), alkaline activator components (NaOH and Na_2SiO_3), the Na_2SiO_3/NaOH ratio, the alkaline-to-binder ratio (A/B), and curing condition (T). The 28-day compressive strength (CS) of geopolymer mortar was defined as the target variable for regression modeling. Prior to training, the dataset was inspected for inconsistencies and organized to ensure numerical stability and compatibility with the selected machine learning algorithm.

4.2 Machine Learning Algorithms

Five regression algorithms with different learning paradigms were employed to capture the inherent nonlinearity of geopolymer systems.

4.2.1 Linear Regression (LR)

Linear regression (LR) is a statistical method widely used to analyze the relationship between input (independent) and output (dependent) variables. Recently, it has been widely implemented in various machine learning libraries and thus has become extremely popular as a machine learning algorithm [41], due to its simplicity and interpretability, it has been one of the most commonly used algorithms in both research and practice. However, its popularity has declined in recent years as predictive accuracy has become more critical. Nevertheless, LR remains an essential baseline model, providing fundamental insights into data behavior and variable relationships [42].

LR can derive linear models in which the dependent variable (y) is a linear function of the independent variables (x). In simple LR, only one independent variable (x) is present, whereas in multiple LR, two or more independent variables (x) are present. In simple LR, the model is of the following form:

$$y = b_o + b_1 x \tag{1}$$

Eq. (1) above represents the equation of a straight line, where b_o and b_1 are the y-intercepts and the slope, respectively. In multiple LR, instead of the line, a plane or a hyperplane is used. The model takes the following form in multiple LR:

$$y = b_o + b_1 x_1 + b_2 x_2 + b_3 x_3 + \ldots b_n x_n \tag{2}$$

In Eq. (2), there are n predictors (x_1, x_2, ..., x_n) [43].

4.2.2 Random Forest Regression (RF)

The random forest algorithm is an ensemble technique. It can be used for both regression and classification. The random forest algorithm uses simple decision trees as the base learners [44]. The training and modeling process for the RF method is shown in Fig. 10 [45]. RF takes decision trees as a basic unit, and a lot of decision trees are integrated to form a random forest [46,47].

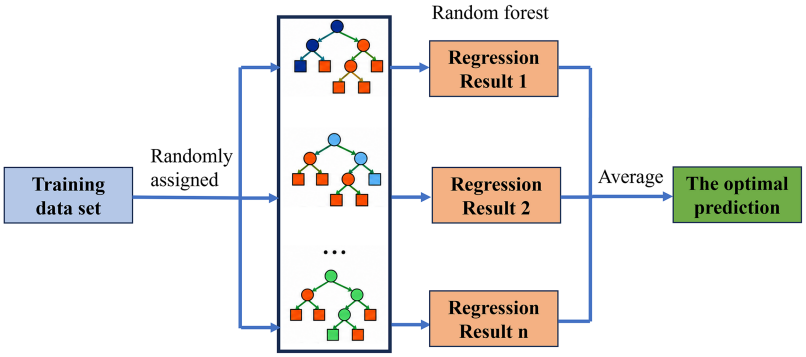

Figure 10: RF modeling flow chart.

4.2.3 Extreme Gradient Boosting (XGBoost)

XGBoost, or extreme gradient boosting, is a popular and powerful ML technique for building supervised regression models [48]. The algorithm is highly efficient and computationally effective. Specifically, a second-order Taylor expansion is used to optimize the loss function, while a regularization term is introduced to control model complexity and avoid overfitting. In addition, XGBoost adopts a block structure for data storage and supports parallel computation. As a forward additive model, XGBoost integrates multiple weak learners into a strong learner through boosting [45].

4.2.4 CatBoost

Categorical Gradient Boosting (CatBoost) is a supervised machine learning (ML) algorithm that employs symmetric decision trees to perform both classification and regression tasks [49]. The CatBoost algorithm is recognized for its strong ability to handle large, complex datasets, producing stable predictions by aggregating multiple model outputs. One of the key advantages of CatBoost is its ability to handle categorical variables effectively while using boosting techniques with a relatively small number of hyperparameters. These characteristics enable efficient model training and significantly reduce computational time during the estimation process [50]. In the CatBoost framework, categorical features are incorporated directly into the learning process, allowing the model to utilize information from the entire dataset. The algorithm initially performs a random permutation (shuffling) of the training samples, which helps minimize prediction bias and prevents target leakage. During the transformation of categorical features into numerical representations, the algorithm sequentially computes the target value for each sample, then assigns corresponding weights and priorities to improve model learning and prediction accuracy [49,51]. In this study, the CatBoost regressor was employed to develop the predictive model, which performs strongly on regression problems, particularly with small- to medium-sized datasets and complex nonlinear relationships. The algorithm was selected due to its ability to reduce prediction bias, improve model stability, and handle feature interactions effectively.

4.2.5 Extra Trees (ETR)

Extra Trees Regressor (ETR), also known as Extremely Randomized Trees or Extra Trees [52], which is an ensemble regression method that builds multiple decision trees and averages their predictions as illustrated in Fig. 11. Unlike Random Forests, it introduces additional randomness by selecting both random data subsets and random split thresholds, rather than optimizing splits. This reduces tree correlation and improves generalization.

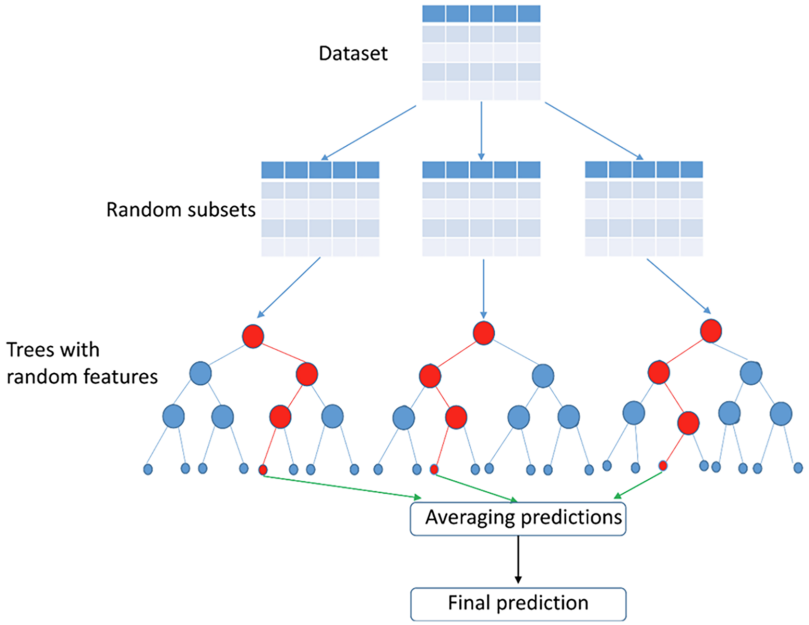

Figure 11: Extra tree model principle.

It is computationally efficient since it avoids split optimization, making it suitable for large, high-dimensional datasets. The increased randomness enhances robustness to overfitting, though it may sometimes lead to less optimal splits. Overall, ETR provides a fast and effective alternative to Random Forests with a balanced bias–variance trade-off [53].

4.3 Dual-Validation Strategy

First, a 10-fold cross-validation (K-Fold CV) was applied [54]. In this method, the dataset was divided into ten equal subsets. During each iteration, nine subsets were used for model training while the remaining subset was used for testing. This process was repeated ten times so that each subset served as a test set once. The average performance across all folds provides a reliable estimate of the model's predictive capability [54].

Second, Monte Carlo was performed to further assess the model's robustness [55]. In this approach, the dataset was randomly shuffled and split into 80% training data and 20% testing data, and this process was repeated 100 times. The mean performance obtained from these repeated random splits provides a more comprehensive evaluation of model stability and reduces the potential influence of random sampling bias [56].

4.4 Performance Evaluation Metrics

The predictive performance of the developed models was evaluated using several statistical indicators commonly employed in regression studies. These metrics included the coefficient of determination (R^2), Root Mean Square Error (RMSE), Mean Absolute Percentage Error (MAPE), Pearson correlation coefficient (r), and the Index of Agreement (IoA).

R^2 measures the proportion of variance in the observed data explained by the model, while RMSE quantifies the magnitude of prediction errors. MAPE provides a normalized measure of prediction accuracy expressed as a percentage. The r evaluates the linear correlation between predicted and experimental values. In addition, the Index of Agreement (IoA) was used to assess the overall agreement between predicted

and observed compressive strength values. These metrics collectively provide a comprehensive evaluation of the predictive capability and reliability of the developed machine learning model. The mathematical formulations of these metrics are given in the following equations:

$$RMSE = \sqrt{\frac{1}{n}\sum_{j=1}^{n}\left(f_{c,j}^{pred} - f_{c,j}^{exp}\right)^2} \tag{3}$$

$$MAPE = \frac{100}{n}\sum_{j=1}^{n}\left|\frac{f_{c,j}^{pred} - f_{c,j}^{exp}}{f_{c,j}^{exp}}\right| \tag{4}$$

$$R^2 = 1 - \frac{\sum_{j=1}^{n}\left(f_{c,j}^{exp} - f_{c,j}^{pred}\right)^2}{\sum_{j=1}^{n}\left(f_{c,j}^{exp} - \overline{f_c^{exp}}\right)^2} \tag{5}$$

$$r = \frac{\sum_{j=1}^{n}\left(f_{c,j}^{pred} - \overline{f_c^{pred}}\right)\left(f_{c,j}^{exp} - \overline{f_c^{exp}}\right)}{\sqrt{\sum_{j=1}^{n}\left(f_{c,j}^{pred} - \overline{f_c^{pred}}\right)^2 \sum_{j=1}^{n}\left(f_{c,j}^{exp} - \overline{f_c^{exp}}\right)^2}} \tag{6}$$

$$IoA = 1 - \frac{\sum_{j=1}^{n}\left(f_{c,j}^{pred} - f_{c,j}^{exp}\right)^2}{\sum_{j=1}^{n}\left(\left|f_{c,j}^{pred} - \overline{f_c^{exp}}\right| + \left|f_{c,j}^{exp} - \overline{f_c^{exp}}\right|\right)^2} \tag{7}$$

In Eqs. (5)–(7), $\overline{f_c^{exp}}$ and $\overline{f_c^{pred}}$ represent the mean values of the 28-day compressive strength recorded experimentally and predicted by the model, respectively. A perfect prediction is achieved when R^2 and IoA are equal to 1, indicating complete agreement between predicted and experimental values. While RMSE and MAPE values approaching 0 indicate minimal prediction error. R^2 and IoA, complementary methods for evaluating model performance, are used to analyze their uncertainty. In addition to conventional statistical metrics, model uncertainty was evaluated using the uncertainty factor (θ), defined as the ratio of the experimentally measured compressive strength to the predicted value.

$$\theta_j = \frac{f_{c,j}^{exp}}{f_{c,j}^{pred}} \tag{8}$$

The distribution of the uncertainty factor is described by its mean and coefficient of variation CoV_θ

$$\overline{\theta} = \frac{1}{n}\sum_{j=1}^{n}\theta_j \tag{9}$$

$$CoV_\theta = \frac{\sigma_\theta}{\overline{\theta}} \tag{10}$$

An ideal predictive model has a mean bias ratio of $\overline{\theta} = 1$, indicating that the model achieves a balanced tendency with neither systematic underestimation nor overestimation. Overall, the complete methodological procedure and validation framework are concisely illustrated in Fig. 12.

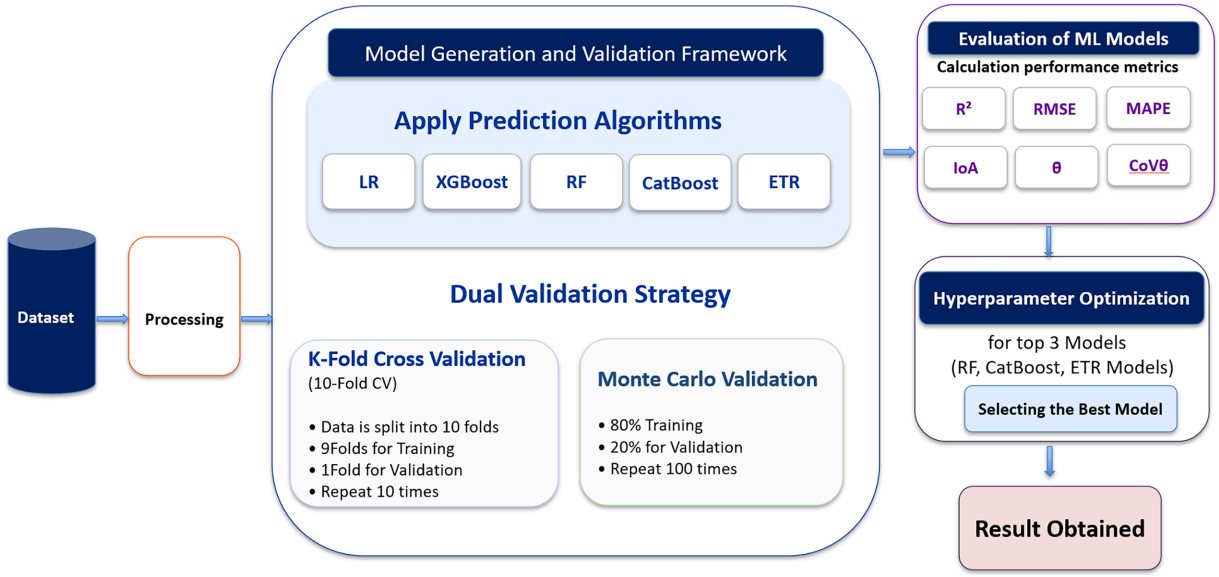

Figure 12: Machine learning framework for predicting compressive strength.

4.5 Model Performance Results and Discussion

The five candidate models, LR, RF, XGBoost, CatBoost, and ETR models were evaluated in three stages: a baseline comparison in their default configuration, Bayesian hyperparameter optimization of the three top performers, and a diagnostic evaluation of the tuned models. All evaluations were conducted using the proposed dual-validation strategy incorporating 10-fold cross-validation and 100-repetition Monte Carlo simulation, The performance of the developed models at each stage of the proposed framework is discussed in detail in the subsequent subsections.

4.5.1 Baseline Performance of Models

All five models were first trained and evaluated in their default configuration to establish a baseline ranking and identify which models would benefit from the additional cost of hyperparameter tuning. The 10-fold cross-validation results (mean ± SD across folds) are reported in Table 3, and the corresponding 100-repetition Monte Carlo results (mean ± SD across repetitions) in Table 4.

Table 3: Baseline 10-fold cross-validation performance of the five candidate models.

Model	RMSE (Mpa)	MAPE (%)	R^2	r	IoA	θ^-	CoV_θ
ETR	5.534 ± 1.711	10.040 ± 3.276	0.902 ± 0.096	0.950 ± 0.026	0.973 ± 0.033	0.997 ± 0.030	0.133 ± 0.042
CatBoost	5.858 ± 1.684	11.762 ± 4.909	0.890 ± 0.082	0.947 ± 0.029	0.968 ± 0.035	0.991 ± 0.035	0.144 ± 0.050
RF	7.273 ± 1.743	14.804 ± 4.544	0.830 ± 0.124	0.913 ± 0.056	0.950 ± 0.042	0.988 ± 0.051	0.183 ± 0.057
XGBoost	7.783 ± 2.554	13.528 ± 3.888	0.806 ± 0.224	0.898 ± 0.102	0.945 ± 0.064	1.016 ± 0.074	0.215 ± 0.076
LR	13.332 ± 3.564	29.466 ± 11.896	0.430 ± 0.338	0.667 ± 0.223	0.797 ± 0.123	1.027 ± 0.136	0.359 ± 0.118

Table 4: Baseline Monte Carlo performance performance of the five candidate models.

Model	RMSE	MAPE (%)	R^2	r	IoA	θ^-	CoVθ
ETR	6.325 ± 1.824	12.268 ± 3.535	0.834 ± 0.125	0.927 ± 0.057	0.953 ± 0.036	0.997 ± 0.041	0.147 ± 0.038
CatBoost	6.827 ± 1.977	14.205 ± 5.043	0.812 ± 0.130	0.920 ± 0.058	0.942 ± 0.042	0.991 ± 0.050	0.167 ± 0.047
RF	7.733 ± 1.899	16.776 ± 4.733	0.755 ± 0.175	0.890 ± 0.077	0.926 ± 0.052	0.986 ± 0.060	0.191 ± 0.047
XGBoost	8.340 ± 2.085	15.606 ± 4.127	0.714 ± 0.193	0.870 ± 0.083	0.919 ± 0.052	1.011 ± 0.058	0.196 ± 0.051
LR	14.058 ± 3.711	30.674 ± 10.298	0.188 ± 0.815	0.641 ± 0.146	0.757 ± 0.099	1.032 ± 0.167	0.339 ± 0.104

ETR consistently emerged as the strongest baseline across both validation protocols, achieving the lowest RMSE (5.534 ± 1.711/6.325 ± 1.824 MPa) and MAPE (10.040 ± 3.276%/12.268 ± 3.535%) and the highest R^2 (0.902 ± 0.096/0.834 ± 0.125). CatBoost ranked second across all metrics, with Random Forest and XGBoost showing more moderate performance and progressively wider gaps relative to ETR. Linear Regression substantially underperformed all nonlinear models; its RMSE was more than twice that of ETR, and its Monte Carlo R^2 (0.188 ± 0.815) indicates that it explains very little of the experimental variance when tested on unseen mixtures. The high SD of LR (R^2 SDs of 0.815 and 0.338) further reflects its instability across different train-test splits, consistent with the strongly nonlinear character of the input-output relationships in nano–silica–modified geopolymer mortar.

The bias ratio (θ^-) was close to unity for the four ensemble models (0.986–1.016), indicating broadly unbiased predictions. ETR additionally exhibited the lowest CoVθ (0.133 ± 0.042/0.147 ± 0.038), confirming the most stable and consistent predictions across the dataset. Based on these baseline results, the three best-performing models, ETR, CatBoost, and RF, were selected for Bayesian hyperparameter optimization.

4.5.2 Bayesian Hyperparameter Optimization

Hyperparameter tuning was performed using Bayesian optimization implemented through the Optuna framework [57] with the Tree-structured Parzen Estimator (TPE) sampler. Bayesian optimization is preferred over grid search and random search because it builds a probabilistic surrogate model of the objective function and concentrates subsequent trials in regions of the search space most likely to improve performance. A total of 200 trials were run per model, with the objective being the mean 10-fold cross-validation R^2 evaluated on the full dataset. A fixed random seed (42) was used throughout to ensure reproducibility. The optimal hyperparameter configurations identified by Optuna are reported in Table 5.

The search spaces are summarized below:

- Extra Trees and Random Forest, the search ranges were: n estimators (100–1000), max features (0.1–1.0), max depth (5–50), min samples split (2–20), min samples leaf (1–10), and ccp alpha (0.0–0.10).
- CatBoost: iterations (500–3000), learning rate (0.001–0.3), depth (3–8), l2 leaf reg (1.0–30.0), min data in leaf (1–30), random strength (0.001–10.0), and bagging temperature (0.0–1.0).

For each tuned model, the optimized configuration was accepted only if it yielded a strictly higher 10-fold CV R^2 than the corresponding default model. All three models satisfied this criterion. As presented in Tables 6 and 7, the tuned configurations were therefore adopted for all subsequent analyses. Performance was reassessed using a set of complementary indicators: coefficient of determination (R^2), root mean square error (RMSE), mean absolute percentage error (MAPE), Pearson correlation coefficient (r), index of agreement (IoA), and the bias-corrected uncertainty statistics (θ^- and CoV_θ) under both 10-fold cross-validation and 100-repetition Monte Carlo simulation.

Table 5: Optimal hyperparameters identified by Bayesian (Optuna TPE).

Hyperparameter	ETR	CatBoost	RF
n_estimators	450	–	600
max_features	0.913	–	0.659
min_samples_split	3	–	2
min_samples_leaf	1	–	1
max_depth	29	–	39
ccp_alpha	0.022	–	0.065
iterations	–	1500	–
learning_rate	–	0.290	–
depth	–	5	–
l2_leaf_reg	–	29.40	–
min_data_in_leaf	–	26	–
random_strength	–	0.063	–
bagging_temperature	–	0.794	–

Table 6: Comparison of default and tuned model performance under 10-fold cross-validation.

Model	Config.	RMSE (MPa)	MAPE (%)	R^2	r	IoA	θ^-	CoV_θ
ETR	Default	5.53	10.04	0.902	0.950	0.973	0.997	0.133
ETR	Tuned	5.43	10.51	0.906	0.952	0.974	0.992	0.134
CatBoost	Default	5.86	11.76	0.890	0.947	0.968	0.991	0.144
CatBoost	Tuned	5.65	11.78	0.898	0.951	0.970	1.001	0.146
RF	Default	7.27	14.80	0.831	0.913	0.950	0.988	0.183
RF	Tuned	6.93	13.09	0.846	0.920	0.957	0.997	0.171

Table 7: Comparison of default and tuned model performance under Monte Carlo simulation.

Model	Config.	RMSE (MPa)	MAPE (%)	R^2	r	IoA	θ^-	CoV_θ
ETR	Default	6.33	12.27	0.834	0.927	0.953	0.997	0.147
ETR	Tuned	6.24	12.13	0.844	0.931	0.955	0.995	0.147
CatBoost	Default	6.83	14.21	0.812	0.920	0.942	0.991	0.167
CatBoost	Tuned	6.77	14.12	0.818	0.922	0.943	0.996	0.168
RF	Default	7.73	16.78	0.755	0.890	0.927	0.986	0.192
RF	Tuned	7.55	15.33	0.766	0.892	0.934	0.999	0.184

Tuning produced consistent, if model-dependent, gains across both protocols. The ETR model exhibited the smallest variation after tuning, with the 10-fold cross-validation R^2 increasing from 0.902 to 0.906 and the Monte Carlo (MC) R^2 improving from 0.834 to 0.844. Similarly, the RMSE decreased from 5.53 to 5.43 MPa under cross-validation and from 6.33 to 6.24 MPa under MC simulation, accompanied by marginal improvements in both Pearson's correlation coefficient (r) and index of agreement (IoA), while the MAPE remained nearly unchanged. CatBoost demonstrated consistent improvements across all evaluation metrics,

with R^2 increasing from 0.890 to 0.898 in cross-validation and from 0.812 to 0.818 in MC simulation. Concurrently, the RMSE decreased from 5.86 to 5.65 MPa and from 6.83 to 6.77 MPa for the respective validation protocols. Among the investigated models, Random Forest exhibited the most pronounced relative improvement following optimization. The R^2 increased from 0.831 to 0.846 under cross-validation and from 0.755 to 0.766 under MC simulation. In parallel, the RMSE decreased from 7.27 to 6.93 MPa and from 7.73 to 7.55 MPa, respectively. Moreover, the MAPE was reduced from 14.80% to 13.09% under cross-validation and from 16.78% to 15.33% under MC simulation. The bias-corrected coefficient of variation (CoVθ) also decreased from 0.183 to 0.171 in cross-validation and from 0.192 to 0.184 in MC simulation, indicating improved predictive consistency and a more uniform model fit. The modest gains for all three tuned models reflect that their default configurations are already well-suited to small-to-medium tabular regression.

4.5.3 Final Tuned Model Selection and Diagnostics

The optimized ETR model was selected as the final predictive model owing to its superior overall performance, characterized by the highest 10-fold cross-validation R^2 (0.906), the lowest RMSE (5.43 MPa), the lowest MAPE, and the strong consistency between cross-validation and Monte Carlo simulation results. These findings indicate the model's robustness and its reliable generalization to unseen geopolymer mortar mixtures. The diagnostic performance of the three optimized models is illustrated in Figs. 13 and 14, where the predicted compressive strengths are compared with the corresponding experimental values under both 10-fold cross-validation and Monte Carlo simulation frameworks.

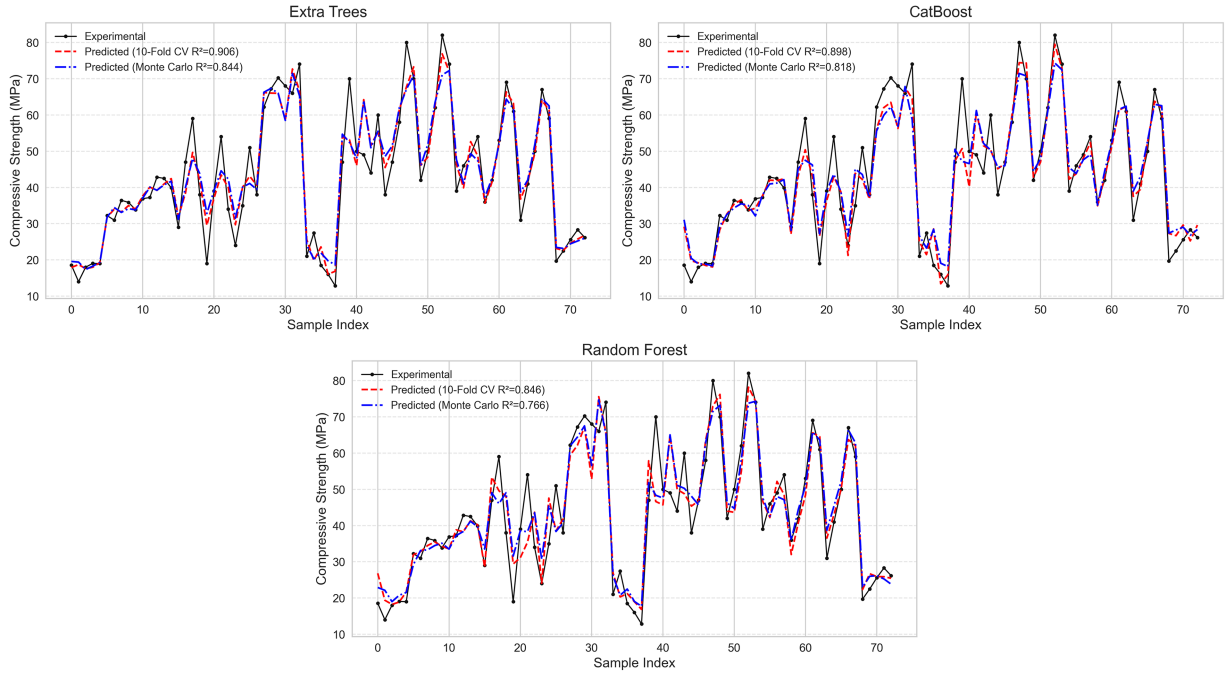

Figure 13: Actual and predicted CS for the ETR, CatBoost, and RF models.

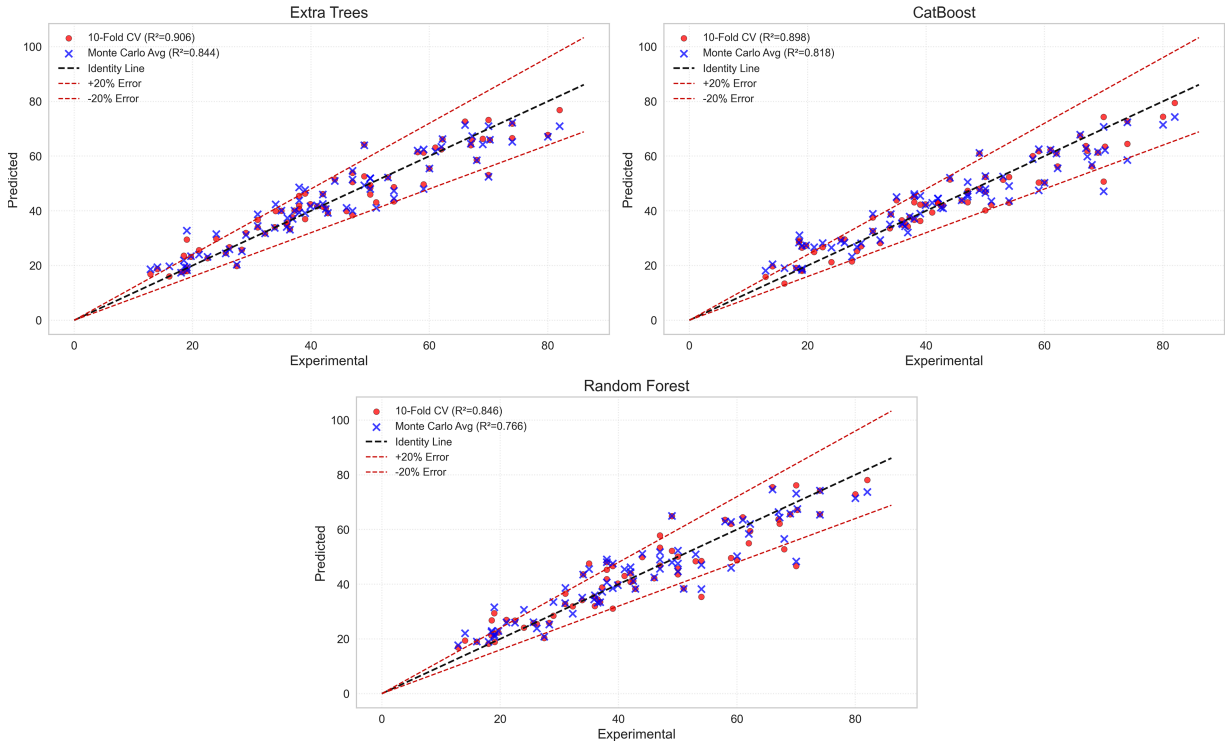

Figure 14: Real data and predicted values of CS based on different algorithms.

The trend plots in Fig. 13 show that the optimized ETR model achieved the closest agreement with the experimental compressive strength values across the full strength range of the dataset (approximately 13–82 MPa). The model successfully captured both the low-strength behaviour of ambient-cured fly ash-dominant mixtures and the high-strength responses of slag and metakaolin-based systems, demonstrating its strong capability to model the nonlinear relationships governing nano-silica–modified geopolymer mortar. CatBoost also exhibited strong predictive performance, although slight smoothing was observed at higher strength levels (>70 MPa). In comparison, RF showed more noticeable smoothing of rapid strength variations, indicating relatively lower sensitivity to localized nonlinear trends within the dataset.

The correlation plots presented in Fig. 14 further confirm the reliability of the developed models, with most predictions clustered near the 1:1 reference line and within ±20% of it. Among the investigated algorithms, the optimized ETR model produced the tightest clustering and lowest dispersion under both 10-fold cross-validation and Monte Carlo simulation, reflecting its superior prediction accuracy and stability. The few observed outliers were mainly associated with mixtures containing extreme nano-silica contents or unusual activator ratios that were sparsely represented in the dataset. Overall, the combined results of the baseline evaluation, Bayesian optimization, and diagnostic analysis support selecting the optimized ETR model as the final predictive model for subsequent analyses.

4.6 Sensitivity Analysis and Feature Interpretation

To further interpret the predictive model, a feature importance analysis was performed using the trained ETR model to quantify the relative influence of key design parameters on the 28-day compressive strength of geopolymer mortar (GPM), as illustrated in Fig. 15. Since Extra Trees is an ensemble tree-based method, the obtained importance values indicate how strongly each input variable contributes to reducing prediction

error within the trained model. Therefore, these results should be interpreted together with the known chemical and microstructural mechanisms governing geopolymerization and strength development.

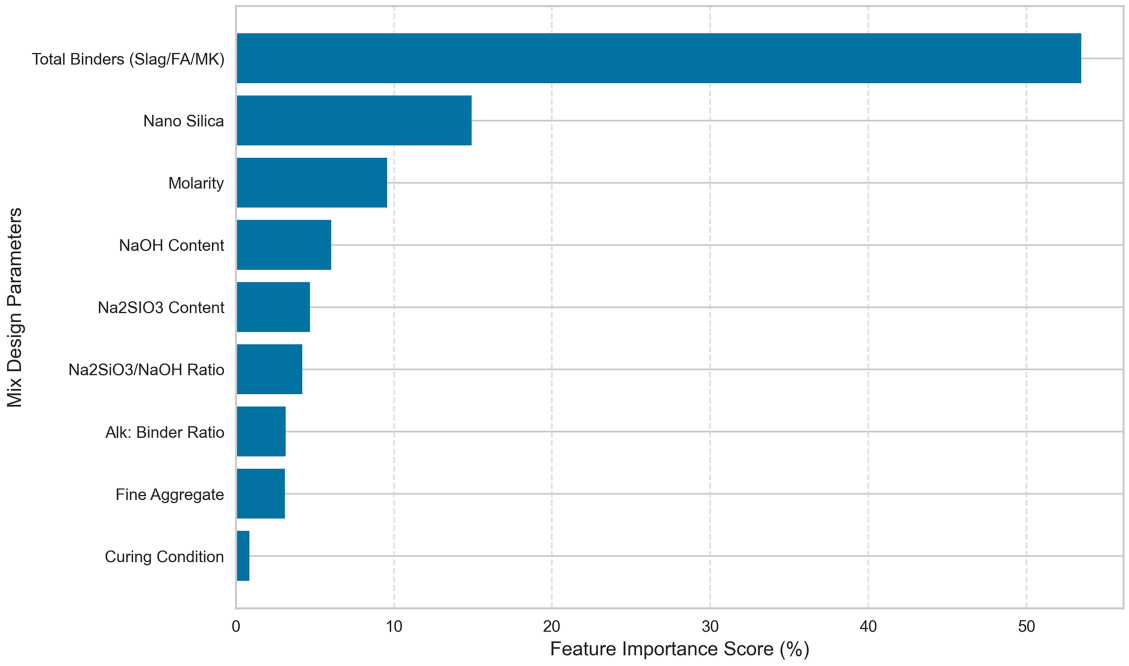

Figure 15: Relative importance of mixture parameters affecting the compressive strength of nano-silica–modified geopolymer mortar.

The results indicate that total binder content (including slag, fly ash, and metakaolin) is the most influential parameter, contributing more than 50% to the prediction of compressive strength. This finding is consistent with previous studies showing that binder composition governs geopolymerization reactions and controls the formation of C–(A)–S–H and N–A–S–H gels responsible for strength development [5]. The compressive strength increased significantly with increasing GGBFS content, highlighting the important role of calcium-rich precursors in enhancing geopolymer reactivity [58,59].

Nano-silica was identified as the second most influential parameter on compressive strength, consistent with its known role in geopolymer and cementitious systems. Due to its extremely fine particle size and high specific surface area, nano-silica acts as a micro-filler, improves particle packing density, provides nucleation sites for gel formation, and supplies additional reactive silica that promotes the development of a denser aluminosilicate gel network [60,61]. However, its influence is dosage-dependent. At optimum contents, nano-silica enhances matrix densification and strength, whereas excessive amounts may cause particle agglomeration, increase water demand, reduce workability, and create weak zones within the matrix. Previous studies similarly reported strength improvement up to an optimum nano-silica dosage followed by strength reduction at higher contents [25,31,32]. Molarity and NaOH content also showed considerable influence, confirming that alkaline concentration strongly affects dissolution of aluminosilicate precursors and reaction kinetics. Similarly, the Na_2SiO_3/NaOH ratio plays a key role in controlling silica availability and gel structure, as reported in prior studies [62].

In contrast, fine aggregate content and curing conditions exhibited comparatively lower importance scores, indicating that, within the investigated range, chemical parameters predominantly govern the compressive strength of geopolymer mortar. This behavior can be attributed to the fact that aggregates

primarily serve as inert fillers within the matrix, contributing to particle packing, dimensional stability, and workability rather than actively contributing to strength development. Consequently, their influence on mechanical performance remains secondary compared to that of the binder system. In alkali-activated materials, the geopolymerization process is fundamentally controlled by the chemistry of the precursor and activator [4,63]. Although heat curing can accelerate reaction kinetics, particularly in low-calcium fly ash systems, the incorporation of slag and nano-silica appears to reduce dependence on elevated-temperature curing by promoting matrix densification and strength development under ambient conditions [64,65].

To further enhance the interpretability of the developed model and provide a more physically meaningful explanation of the observed trends, partial dependence plots (PDPs) were generated for key variables, including nano-silica content, NaOH molarity, and slag content, as shown in Fig. 16. Unlike marginal plots, which reflect only pairwise relationships, PDPs illustrate the isolated effect of each variable on the predicted compressive strength while averaging out the influence of all other input parameters. This enables a more reliable interpretation of nonlinear interactions captured by the optimized ETR model.

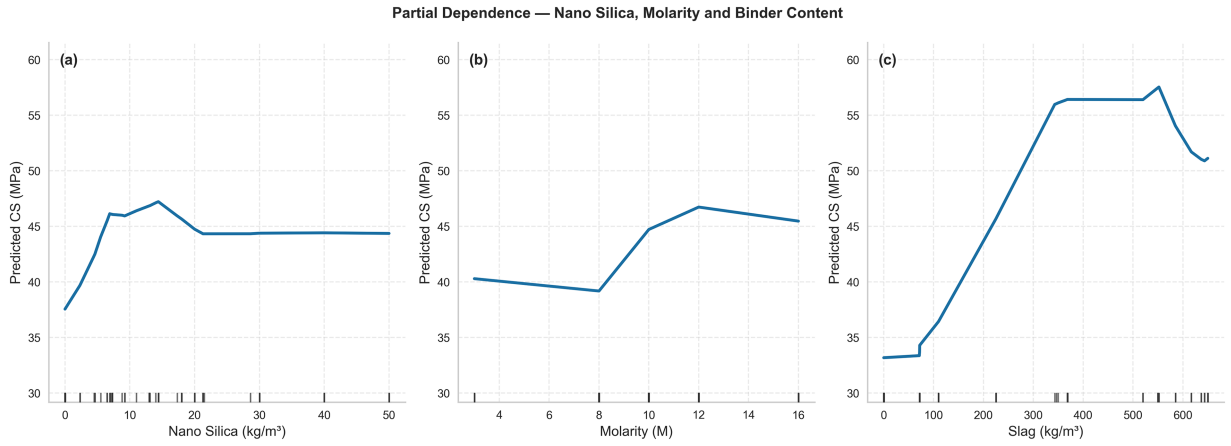

Figure 16: Partial dependence plots for (**a**) nano-silica content, (**b**) molarity of NaOH, and (**c**) slag content, derived from the tuned ETR model.

Fig. 16a indicates that nano-silica exhibits a nonlinear influence on compressive strength, with strength initially increasing at low dosages before stabilizing or slightly decreasing beyond the optimum range, likely due to nanoparticle agglomeration. Fig. 16b shows that increasing NaOH molarity enhances compressive strength up to approximately 10–12 M, after which the beneficial effect becomes less pronounced. Similarly, Fig. 16c confirms the strong positive contribution of slag content, with compressive strength increasing substantially up to approximately 400–500 kg/m^3 before gradually approaching a plateau.

5 Implementation and Practical Application

A user-friendly open-access web application was developed to predict the 28-day compressive strength of geopolymer mortar using the Extra Trees (ET) model, which demonstrated the highest predictive performance among all evaluated models. The tool enables users to input key mixture design parameters, including Molarity (M), Fly ash, Slag, Metakaolin, Fine Aggregate, Nano-Silica content, NaOH, Na_2SiO_3, the Na_2SiO_3/NaOH ratio, the Alkaline-to-Binder ratio, and curing condition. Based on these inputs, the trained model provides an instant prediction of compressive strength.

The application features an interactive interface that allows researchers and engineers to easily adjust mixture parameters and obtain rapid strength estimates without requiring machine-learning expertise. Additionally, the platform displays model validation results from both 10-fold and Monte Carlo cross-validation (100 repetitions), providing transparency into the predictive reliability of the developed model.

A screenshot of the web interface is shown in Fig. 17. The application's source code is publicly available at https://github.com/briarpt-rgb/geopolymer-mortar-strength-predictor, and the online prediction tool is accessible at https://geopolymer-mortar-strength-predictor.streamlit.app/.

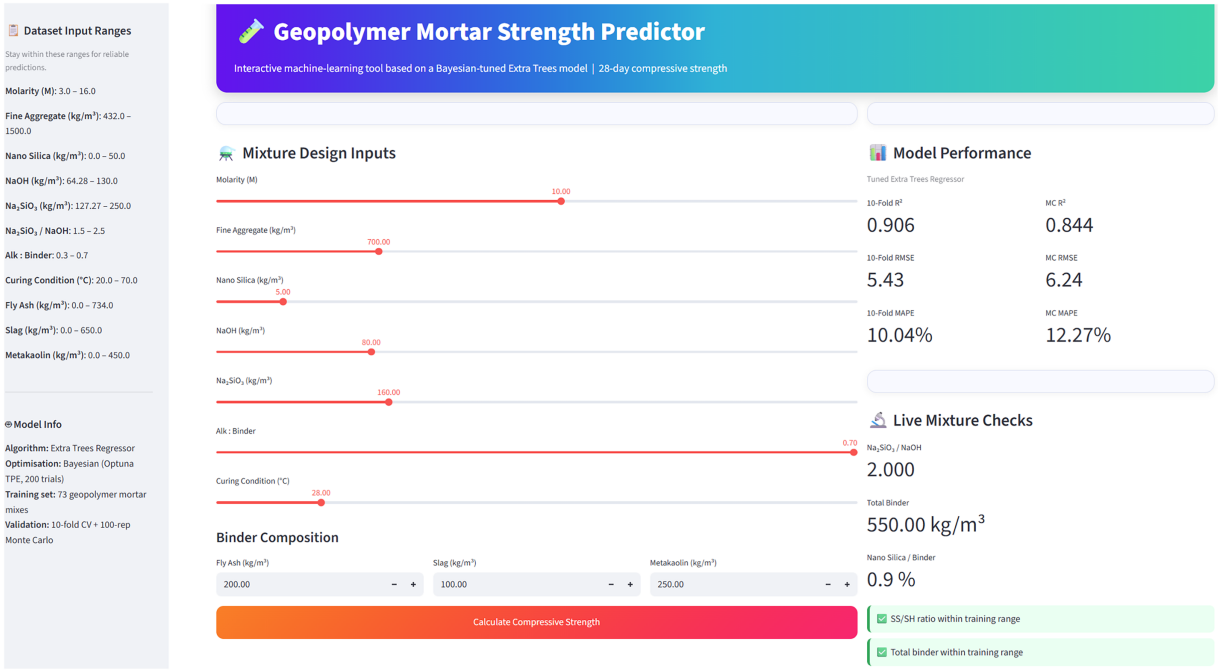

Figure 17: Screenshot of the developed compressive strength prediction tool.

6 Conclusions

This study developed and evaluated machine learning models to predict the 28-day compressive strength of nano-silica-modified hybrid geopolymer mortar using a dataset of 73 mixtures compiled from the literature. Five machine learning algorithms, including LR, RF, CatBoost, XGBoost, and ETR, were comparatively assessed using 10-fold cross-validation and Monte Carlo simulation. Based on the obtained results, the following conclusions can be drawn:

- The three best-performing models, namely ETR, CatBoost, and Random Forest, were further refined through Bayesian hyperparameter optimization using the Optuna TPE sampler over 200 trials. Among all evaluated models, the optimized ETR achieved the highest predictive accuracy, with R^2 values of 0.906 and 0.844 under 10-fold cross-validation and Monte Carlo simulation, respectively, whereas the baseline LR model exhibited the lowest predictive capability. Hyperparameter optimization produced consistent improvements across the ensemble models, with Random Forest showing the greatest relative enhancement: the R^2 value increased from 0.831 to 0.846 and the MAPE decreased from 14.80% to 13.09% under 10-fold cross-validation. These results demonstrate the effectiveness of systematic optimization and confirm the ETR model's superior ability to capture the complex nonlinear behavior governing geopolymer mortar strength.

- The reliability and robustness of the optimized ETR model were further confirmed through bias and error analysis. The model exhibited negligible systematic bias, with θ^{-} values of 0.992 and 0.995 under 10-fold cross-validation and Monte Carlo simulation, respectively. Moreover, the low CoVθ values (0.134 and 0.147), high agreement indices (r = 0.952 and 0.931; IoA = 0.974 and 0.955), and relatively low prediction errors (RMSE = 5.43 and 6.24 MPa; MAPE = 10.51% and 12.13%) demonstrate stable, accurate, and consistent predictive performance across both validation strategies.
- Feature importance analysis of the Extra Trees Regressor (ETR) model revealed that precursor binder composition (slag, fly ash, and metakaolin contents) was the dominant factor governing the 28-day compressive strength of geopolymer mortar, contributing more than 50% of the total model importance. Nano-Silica dosage ranked as the second most influential parameter at approximately 15%, followed by NaOH molarity and alkaline activator content. In contrast, the alkaline-to-binder ratio, Na_2SiO_3/NaOH ratio, fine aggregate content, and curing conditions exhibited comparatively smaller contributions. These findings are physically interpretable and consistent with the established chemical and microstructural mechanisms of geopolymerization, thereby supporting the reliability and robustness of the model predictions.
- Finally, an open-access, user-friendly web tool application was developed as a practical tool for estimating 28-day compressive strength of geopolymer mortar modified with nano silica based on mixture design parameters, enabling rapid assessment for researchers and practitioners.

Limitations and Future Work Recommendations

A key limitation of this study is that the model is developed from a small size dataset (73 mixes), reflecting the current scarcity of available data on nano-silica–modified geopolymer systems.

Although the use of dual validation approaches, including 10-fold cross-validation and Monte Carlo simulation, enhances the internal reliability of the developed models, the absence of independent external validation remains a limitation. Future studies should incorporate larger and externally validated experimental datasets to further evaluate and improve the generalizability and robustness of the proposed prediction framework.

Acknowledgement: Briar Esmail acknowledges the support from the Portuguese Science Foundation (FCT) through the PhD individual grant with the reference 2024.05965.BDANA.

Funding Statement: The authors received no specific funding for this study.

Author Contributions: The authors confirm their contribution to the paper: study conception and design: Soran Manguri, Briar Esmail, Kasim Mermerdaş, Ahmed Manguri, Data collection: Soran Manguri, Ahmed Manguri, Data analysis: Soran Manguri, Briar Esmail, Ahmed Manguri, Draft manuscript preparation: Soran Manguri, Briar Esmail, Kasim Mermerdaş, Ahmed Manguri. All authors reviewed and approved the final version of the manuscript.

Availability of Data and Materials: Data available on request from the authors. The data that support the findings of this study are available from the First and the Corresponding Authors [Soran Manguri, and Ahmed Manguri], upon reasonable request.

Ethics Approval: Not applicable.

Conflicts of Interest: The funders had no role in the design of the study; in the collection, analyses, or interpretation of data; in the writing of the manuscript; or in the decision to publish the results.

Abbreviations

The following abbreviations are used in this manuscript:

C-A-S-H	Calcium-alumino-silicate-hydrate
N–A–S–H	Sodium aluminosilicate hydrate
GPM	Geopolymer mortar
AAM	Alkali Activated Mortar
Ns	Nano-silica
CS	Compressive strength
R^2	Coefficient of determination
RMSE	Root mean squared error
MAE	Mean absolute error
SI	Scatter index
ML	Machine Learning
LR	Linear regression
RF	Random Forest
XGBoost	Extreme Gradient Boosting
ETR	Extra Trees Regressor
NLR	Nonlinear regression
MLR	Multi-logistic regression
ANN	Artificial neural network
TPE	Tree-structured Parzen Estimator
CV	Cross Validation
MC	Monte Carlo
A/B	Alkaline solution to binder ratio
SH	Sodium hydroxide
SS	Sodium silicate
SS/SH	Sodium silicate to sodium hydroxide ratio
M	Molarity of sodium hydroxide
FA	Fine aggregate
T	Curing temperature
A	Geopolymer mortar specimens' ages
B	Binder content
Nm	Nanometer
NPs	Nanoparticles

References

1. Scrivener KL, John VM, Gartner EM. Eco-efficient cements: potential economically viable solutions for a low-CO_2 cement-based materials industry. Cem Concr Res. 2018;114(5):2–26. doi:10.1016/j.cemconres.2018.03.015.
2. Habert G, Miller SA, John VM, Provis JL, Favier A, Horvath A, et al. Environmental impacts and decarbonization strategies in the cement and concrete industries. Nat Rev Earth Environ. 2020;1(11):559–73. doi:10.1038/s43017-020-0093-3.
3. Andrew RM. Global CO_2 emissions from cement production. Earth Syst Sci Data. 2018;10(1):195–217. doi:10.5194/essd-10-195-2018.
4. John L, Provis JV. Alkali activated materials. Berlin/Heidelberg, Germany: Springer; 2014.
5. Davidovits J. Geopolymer chemistry and applications. Saint-Quentin, France: Geopolymer Institute; 2008.
6. Duxson P, Provis JL, Lukey GC, van Deventer JSJ. The role of inorganic polymer technology in the development of 'green concrete'. Cem Concr Res. 2007;37(12):1590–7. doi:10.1016/j.cemconres.2007.08.018.
7. Mermerdaş K, Manguri S, Nassani DE, Oleiwi SM. Effect of aggregate properties on the mechanical and absorption characteristics of geopolymer mortar. Eng Sci Technol Int J. 2017;20(6):1642–52. doi:10.1016/j.jestch.2017.11.009.

8. Assi L, Carter K, Deaver E, Anay R, Ziehl P. Sustainable concrete: building a greener future. J Clean Prod. 2018;198:1641–51. doi:10.1016/j.jclepro.2018.07.123.
9. Wardhono A, Law DW, Molyneaux TCK. Long term performance of alkali activated slag concrete. J Adv Concr Technol. 2015;13(3):187–92. doi:10.3151/jact.13.187.
10. Shrestha R, Baweja D, Neupane K, Chalmers D, Sleep P. Mechanical properties of geopolymer concrete: applicability of relationships defined by AS 3600. In: Proceedings of the Concrete Institute of Australia-Biennial Conference; 2013 Oct 16–18; Gold Coast, Australia.
11. Rovnaník P. Effect of curing temperature on the development of hard structure of metakaolin-based geopolymer. Constr Build Mater. 2010;24(7):1176–83. doi:10.1016/j.conbuildmat.2009.12.023.
12. Davidovits J. High-alkali cements for 21st century concretes. Special Publication. 1994;144:383–98. doi:10.14359/4523.
13. Provis JL. Alkali-activated materials. Cem Concr Res. 2018;114:40–8. doi:10.1016/j.cemconres.2017.02.009.
14. Komnitsas K, Zaharaki D. Geopolymerisation: a review and prospects for the minerals industry. Miner Eng. 2007;20(14):1261–77. doi:10.1016/j.mineng.2007.07.011.
15. Nath P, Sarker P. Effect of fly ash on the durability properties of high strength concrete. Procedia Eng. 2011;14(2):1149–56. doi:10.1016/j.proeng.2011.07.144.
16. Rangan BV, Hardjito D, Wallah SE, Sumajouw DM. Studies on fly ash-based geopolymer concrete. In: Proceedings of the World Congress Geopolymer; 2005 Jun 29–Jul 1; Saint-Quentin, France.
17. Xu H, Van Deventer JSJ. The geopolymerisation of alumino-silicate minerals. Int J Miner Process. 2000;59(3):247–66. doi:10.1016/S0301-7516(99)00074-5.
18. Palomo A, Grutzeck MW, Blanco MT. Alkali-activated fly ashes: a cement for the future. Cem Concr Res. 1999;29(8):1323–9. doi:10.1016/S0008-8846(98)00243-9.
19. Bakharev T. Thermal behaviour of geopolymers prepared using class F fly ash and elevated temperature curing. Cem Concr Res. 2006;36(6):1134–47. doi:10.1016/j.cemconres.2006.03.022.
20. Deb PS, Nath P, Sarker PK. The effects of ground granulated blast-furnace slag blending with fly ash and activator content on the workability and strength properties of geopolymer concrete cured at ambient temperature. Mater Des 1980–2015. 2014;62:32–9. doi:10.1016/j.matdes.2014.05.001.
21. Sanchez F, Sobolev K. Nanotechnology in concrete—a review. Constr Build Mater. 2010;24(11):2060–71. doi:10.1016/j.conbuildmat.2010.03.014.
22. Quercia G, Brouwers H. Application of nano-silica (nS) in concrete mixtures. In: Proceedings of the 8th fib International PhD Symposium in Civil Engineering Lyngby; 2010 Jun 20–23; Lyngby, Denmark.
23. Ma L, Sun M, Yang J, Dai Q. Nanosilica-enhanced geopolymer cementitious materials: mechanistic insights from experimental and computational simulations. J Build Eng. 2024;98(8):111098. doi:10.1016/j.jobe.2024.111098.
24. Zhang P, Han X, Guo J, Hu S. High-temperature behavior of geopolymer mortar containing nano-silica. Constr Build Mater. 2023;364(6):129983. doi:10.1016/j.conbuildmat.2022.129983.
25. Rathinam K, Sakthivel S, Vigneshwaran SP, Vinayagamoorthy M, Naveen Kumar U. Properties of nano silica modified cement less geopolymer composite mortar using fly ash and GGBS. Mater Today Proc. 2022;62(1):535–42. doi:10.1016/j.matpr.2022.03.589.
26. Zhang P, Zhang X, Yuan P, Hu S. Performance optimization of geopolymer mortar blending in nano-SiO_2 and PVA fiber based on set pair analysis. E Polym. 2023;23(1):20230015. doi:10.1515/epoly-2023-0015.
27. Chou JS, Tsai CF, Pham AD, Lu YH. Machine learning in concrete strength simulations: multi-nation data analytics. Constr Build Mater. 2014;73(5):771–80. doi:10.1016/j.conbuildmat.2014.09.054.
28. Ahmed HU, Abdalla AA, Mohammed AS, Mohammed AA, Mosavi A. Statistical methods for modeling the compressive strength of geopolymer mortar. Materials. 2022;15(5):1868. doi:10.3390/ma15051868.
29. Ahmed HU, Mohammed AS, Faraj RH, Qaidi SMA, Mohammed AA. Compressive strength of geopolymer concrete modified with nano-silica: experimental and modeling investigations. Case Stud Constr Mater. 2022;16(2):e01036. doi:10.1016/j.cscm.2022.e01036.
30. Karaci A, Yaprak H, Ozkaraca O, Demir I, Simsek O. Estimating the properties of ground-waste-brick mortars using DNN and ANN. Comput Model Eng Sci. 2019;118(1):207–28. doi:10.31614/cmes.2019.04216.

31. Adak D, Sarkar M, Mandal S. Effect of nano-silica on strength and durability of fly ash based geopolymer mortar. Constr Build Mater. 2014;70(1):453–9. doi:10.1016/j.conbuildmat.2014.07.093.
32. Deb PS, Sarker PK, Barbhuiya S. Sorptivity and acid resistance of ambient-cured geopolymer mortars containing nano-silica. Cem Concr Compos. 2016;72(9):235–45. doi:10.1016/j.cemconcomp.2016.06.017.
33. Prakasam G, Murthy AR, Saffiq Reheman M. Mechanical, durability and fracture properties of nano-modified FA/GGBS geopolymer mortar. Mag Concr Res. 2020;72(4):207–16. doi:10.1680/jmacr.18.00059.
34. Dheyaaldin MH, Ali Mosaberpanah M, Alzeebaree R. Performance of fiber-reinforced alkali-activated mortar with/without nano silica and nano alumina. Sustainability. 2022;14(5):2527. doi:10.3390/su14052527.
35. Hussein TA, Dheyaaldin MH, Ali Mosaberpanah M, Ahmed YMS, Mohammed HA, Omer RR, et al. Chemical resistance of alkali-activated mortar with nano silica and polypropylene fiber. Constr Build Mater. 2023;363:129847. doi:10.1016/j.conbuildmat.2022.129847.
36. Selvarajan D, Paramasivam SK. Experimental and FEA analysis on flexural behavior of a ferrocement slab using GGBS and Nano Silica. Matéria. 2023;28(4):e20230205. doi:10.1590/1517-7076-rmat-2023-0205.
37. Gökçegöz Y, Uysal M, Aygun BF. Effect of Nano-SiO_2 on electrical cured metakaolin-granulated blast furnace slag based geopolymers with fiber addition. In: Proceedings of the 15th International PhD Symposium in Civil Engineering; 2024 Aug 28–30; Budapest, Hungary.
38. Seenipeyathevar MS, Shanmugam B, Ramakrishnan A, Battena KR, Ramasamy V, Murugesan V. A comprehensive study on advanced strategies to improve the performance, durability, and flexible behavior of cementitious materials. Matéria. 2024;29(3):e20240217. doi:10.1590/1517-7076-rmat-2024-0217.
39. Kamal HM, Kadhim MJ, Hasan LM. Impact of nanoparticles on the performance of metakaolin-based geopolymer composites. J Mech Behav Mater. 2025;34(1):20250072. doi:10.1515/jmbm-2025-0072.
40. Ahmed HU, Mohammed AS, Mohammed AA, Faraj RH. Systematic multiscale models to predict the compressive strength of fly ash-based geopolymer concrete at various mixture proportions and curing regimes. PLoS One. 2021;16(6):e0253006. doi:10.1371/journal.pone.0253006.
41. Montgomery DC, Peck EA, Vining GG. Introduction to linear regression analysis. Hoboken, NJ, USA: John Wiley & Sons, Inc.; 2021.
42. Mirzahosseini M, Jiao P, Barri K, Riding KA, Alavi AH. New machine learning prediction models for compressive strength of concrete modified with glass cullet. Eng Comput. 2019;36(3):876–98. doi:10.1108/ec-08-2018-0348.
43. Gayathri R, Rani SU, Čepová L, Rajesh M, Kalita K. A comparative analysis of machine learning models in prediction of mortar compressive strength. Processes. 2022;10(7):1387. doi:10.3390/pr10071387.
44. Biau G, Scornet E. A random forest guided tour. TEST. 2016;25(2):197–227. doi:10.1007/s11749-016-0481-7.
45. Fei Z, Liang S, Cai Y, Shen Y. Ensemble machine-learning-based prediction models for the compressive strength of recycled powder mortar. Materials. 2023;16(2):583. doi:10.3390/ma16020583.
46. Genuer R, Poggi JM, Tuleau-Malot C, Villa-Vialaneix N. Random forests for big data. Big Data Res. 2017;9(2):28–46. doi:10.1016/j.bdr.2017.07.003.
47. Biau G. Analysis of a random forests model. J Mach Learn Res. 2012;13:1063–95.
48. Chen T, Guestrin C. XGBoost: a scalable tree boosting system. In: Proceedings of the 22nd ACM SIGKDD International Conference on Knowledge Discovery and Data Mining; 2016 Aug 13–17; San Francisco, CA, USA. p. 785–94. doi:10.1145/2939672.2939785.
49. Prokhorenkova L, Gusev G, Vorobev A, Dorogush AV, Gulin A. CatBoost: unbiased boosting with categorical features. Adv Neural Inf Process Syst. 2018;31:1–11.
50. Bentéjac C, Csörgő A, Martínez-Muñoz G. A comparative analysis of gradient boosting algorithms. Artif Intell Rev. 2021;54(3):1937–67. doi:10.1007/s10462-020-09896-5.
51. Eid MM, Alhussan AA, Mattar EA, Khodadadi N, El-Kenawy ESM. Concrete strength prediction using machine learning and somersaulting spider optimizer. Comput Model Eng Sci. 2026;146(1):1–10. doi:10.32604/cmes.2025.073555.
52. Geurts P, Ernst D, Wehenkel L. Extremely randomized trees. Mach Learn. 2006;63(1):3–42. doi:10.1007/s10994-006-6226-1.

53. Hilloulin B, Umunnakwe R. Machine learning-aided prediction of shrinkage in modern concrete: focus on mix proportions and SCMs. J Build Eng. 2024;98:111410. doi:10.1016/j.jobe.2024.111410.
54. Kohavi R. A study of cross-validation and bootstrap for accuracy estimation and model selection. In: International Joint Conference on Artificial Intelligence; 1995 Aug 20–25; Montreal, QC, Canada.
55. Metropolis N, Ulam S. The Monte Carlo method. J Am Stat Assoc. 1949;44(247):335–41. doi:10.1080/01621459.1949.10483310.
56. Arlot S, Celisse A. A survey of cross-validation procedures for model selection. Statist Surv. 2010;4:40–79. doi:10.1214/09-ss054.
57. Akiba T, Sano S, Yanase T, Ohta T, Koyama M. Optuna: a next-generation hyperparameter optimization framework. In: Proceedings of the 25th ACM SIGKDD International Conference on Knowledge Discovery & Data Mining; 2019 Aug 4–8; Anchorage, AK, USA. p. 2623–31. doi:10.1145/3292500.3330701.
58. Aslan S, Erkan İH. The effects of fly ash, blast furnace slag, and limestone powder on the physical and mechanical properties of geopolymer mortar. Appl Sci. 2024;14(2):553. doi:10.3390/app14020553.
59. Sitarz M, Hager I, Choińska M. Evolution of mechanical properties with time of fly-ash-based geopolymer mortars under the effect of granulated ground blast furnace slag addition. Energies. 2020;13(5):1135. doi:10.3390/en13051135.
60. Seloğlu M, Tanyıldızı H, Öncü ME. An investigation of the strength properties of fly ash and metakaolin-based geopolymer mortars containing multi-wall carbon nanotube, nano silica, and nano zinc. Bitlis Eren Üniversitesi Fen Bilimleri Dergisi. 2023;12(3):842–52. doi:10.17798/bitlisfen.1323858.
61. Zhang G, Zhang P, Guo J, Hu S. Effects of PVA fibers and nano-SiO_2 on rheological properties of geopolymer mortar. Nanotechnol Rev. 2024;13(1):20240103. doi:10.1515/ntrev-2024-0103.
62. Al Bakri Abdullah MM, Kamarudin H, Bnhussain M, Ismail KN, Rafiza AR, Zarina Y. The relationship of NaOH molarity, Na_2SiO_3/NaOH ratio, fly ash/alkaline activator ratio, and curing temperature to the strength of fly ash-based geopolymer. Adv Mater Res. 2011;328–330:1475–82. doi:10.4028/www.scientific.net/amr.328-330.1475.
63. Neville AM. Properties of concrete. New York, NY, USA: Pearson; 2011.
64. Işıkdağ B, Mutlu HA. Durability of non-heat-cured geopolymer mortars containing metakaolin and ground granulated blast furnace slag. Minerals. 2024;14(8):776. doi:10.3390/min14080776.
65. Özkılıç YO, Mohamud MA, Yılmaz F, Alasiri MR, Çelik Aİ. The relationship of curing methods and curing temperatures with NaOH molarity and their effects on the behavior of geopolymer concrete. Sci Rep. 2026;16(1):8346. doi:10.1038/s41598-026-39478-4.